Deciphering cometary outbursts: Linking gas composition changes to trigger mechanisms

Daniel Müller, Kathrin Altwegg, Jean-Jacques Berthelier, Michael Combi, Johan de Keyser, Stephen Fuselier, Philippe Garnier, Nora Hänni, Urs Mall, Martin Rubin, et al.

Monthly Notices of the ROYAL ASTRONOMICAL SOCIETY

MNRAS **529,** 2763–2776 (2024) https://doi.org/10.1093/mnras/stae622
Advance Access publication 2024 February 29

Deciphering cometary outbursts: linking gas composition changes to trigger mechanisms

Daniel R. Müller [1]★ Kathrin Altwegg [1] Jean-Jacques Berthelier [2] Michael R. Combi [3] Johan De Keyser [4] Stephen A. Fuselier [5,6] Philippe Garnier,[7] Nora Hänni [1] Urs Mall [8] Martin Rubin [1] Susanne F. Wampfler [9] and Peter Wurz [1,9]

[1]*Space Research and Planetary Sciences, Physics Institute, University of Bern, Sidlerstrasse 5, CH-3012 Bern, Switzerland*
[2]*Laboratoire Atmosphères, Milieux, Observations Spatiales (LATMOS), 4 Avenue de Neptune, F-94100 Saint-Maur, France*
[3]*Department of Climate and Space Sciences and Engineering, University of Michigan, 2455 Hayward, Ann Arbor, MI 48109, USA*
[4]*Royal Belgian Institute for Space Aeronomy, BIRA-IASB, Ringlaan 3, B-1180 Brussels, Belgium*
[5]*Space Science Directorate, Southwest Research Institute, 6220 Culebra Rd., San Antonio, TX 78228, USA*
[6]*Department of Physics and Astronomy, The University of Texas at San Antonio, San Antonio, TX 78249, USA*
[7]*IRAP, Université de Toulouse, CNRS, CNES, UPS, 9 Avenue du Colonel Roche, F-31028 Toulouse, France*
[8]*Max-Planck Institute for Solar System Research, Justus-von-Liebig-Weg 3, D-37077 Göttingen, Germany*
[9]*Center for Space and Habitability, University of Bern, Gesellschaftsstrasse 6, CH-3012 Bern, Switzerland*

Accepted 2024 February 27. Received 2024 February 27; in original form 2024 January 10

ABSTRACT

Dust and gas outbursts are recurrent cometary phenomena, playing a crucial role in shaping the coma. Proposed outburst trigger mechanisms include cliff collapse, pressure pockets, and amorphous-to-crystalline phase transition of water ice; however, the underlying processes remain inadequately understood. In this study, we analyse *Rosetta*/ROSINA data from multiple outbursts on comet 67P/Churyumov-Gerasimenko and present the evolution of the gas composition in the comet's coma during outburst events. We distinguish two distinct categories of cometary outbursts on the comet: water-driven events characterized by rapid (minutes to hours) changes in coma composition, and CO_2-driven events displaying a slow, prolonged (hours to days) increase in highly volatile species. We tentatively associate these different gas composition patterns with different trigger mechanisms. Exposure of fresh ice due to cliff collapse leads to a notable water enhancement, while most perihelion outbursts coincide with substantial density increases of CO_2. We propose that these CO_2-driven events originate from subsurface gas-filled cavities, whose walls are suggested to have been sealed by earlier refreezing of CO_2 migrating from warmer spots, hence increasing the cavity pressure required to burst.

Key words: instrumentation: detectors – methods: data analysis – comets: general – comets: individual: 67P/Churyumov-Gerasimenko.

1 INTRODUCTION

Comet outbursts are universal and recurring phenomena. Hughes (1975, 1991) demonstrated that outbursts are common events and occur episodically on all comets. These transient phenomena, marked by sudden mass ejections, play a crucial role in understanding the evolutionary processes shaping the surface of comets, while offering valuable insights into the physical properties of their nuclei (Hughes 1991). Despite extensive research (e.g. Lin et al. 2009; Ishiguro et al. 2014, 2016; Shinnaka et al. 2018; Wierzchos & Womack 2020; Bockelée-Morvan et al. 2022) questions persist about their underlying nature and triggering mechanisms.

Prialnik, A'Hearn & Meech (2008) proposed a mechanism to explain short-lived outbursts observed during the Deep Impact mission on 9P/Tempel 1. They suggested that solar radiation generates a heat wave, causing ice sublimation beneath the dust layer. This vapour migrates towards the surface, but refreezes before it gets there because, due to the slow process, by the time the heatwave reaches the ice, the area has moved out of the sunlight, causing the temperature to drop. The subsequent sunrise leads to the evaporation of the newly formed ice within the dust layer. Belton et al. (2008) proposed a similar mechanism for outbursts on the same comet, but independent of direct solar illumination. In addition to the transport of H_2O vapour described by Prialnik, A'Hearn & Meech (2008), they propose thermal stresses and subsurface effects to control the initiation of outbursts.

In contrast to the relatively small outbursts on 9P/Tempel 1, a massive outburst occurred on 17P/Holmes in 2007. The substantial gas production rate during this event is suggested to be the result of either the explosive sublimation of a highly volatile region in the comet's surface layer or a transient outgassing event involving the entire nucleus (Lin et al. 2009). Moreover, Bockelée-Morvan et al. (2022) identified a correlation between coma brightness and CO gas production during outbursts on comet 29P/Schwassmann-Wachmann 1 (29P) in 2007 and 2010. Following these events, the

★ E-mail: daniel.mueller@unibe.ch

CO gas production rate remained elevated for several days. Their findings, coupled with the slow rotation of 29P, led to the suggestion that fractures or pits on the nucleus surface may act as efficient heat traps, enhancing outgassing compared to a uniformly illuminated surface. Similarly, for outburst events observed on 29P between 2018 and 2021, the driving activity was suggested to come mostly from CO outgassing (Lin 2023). Conversely, Wierzchos & Womack (2020) observed dust outbursts on the same comet not correlated to CO outgassing. They state that this may hint at CO being intimately mixed with the dust component in the nucleus, or if CO is primarily released through a porous material.

Hughes (1975) summarized potential outburst triggering mechanisms, including pressure release from gas pockets, explosive radicals, amorphous-to-crystalline ice transition, impact cratering by boulders, break-up of nucleus, and nuclear crushing. They also suggested that there is not just one single mechanism triggering cometary outbursts.

The *Rosetta* mission provided unique insights into comet 67P/Churyumov-Gerasimenko (hereafter 67P), rendering it the best-studied comet to date, and significantly advanced our understanding of these objects (e.g. Altwegg et al. 2015; Sierks et al. 2015; Fulle et al. 2016; Altwegg, Balsiger & Fuselier 2019; Thomas et al. 2019; Hänni et al. 2022). 67P displayed numerous localized dust and gas jet features (e.g. Agarwal et al. 2017; Bockelée-Morvan et al. 2017; Lin et al. 2017; Schmitt et al. 2017), offering a unique opportunity to investigate these outburst phenomena across extended time frames and in exceptional detail.

Skorov et al. (2016) formulated a physical model to explain outbursts observed within fractured terrains on comet 67P near perihelion. They postulated that as the stresses on the nucleus increased during the perihelion approach, pre-existing cracks or fractures would deepen, reaching into underlying material rich in highly volatile ices in equilibrium with the surrounding environment. The sudden propagation of these fractures would trigger a violent sublimation of the highly volatile ices. Their proposed mechanism is independent of the solar illumination history of specific regions or the presence of large, sealed cavities within the nucleus. A parallel explanation was offered by Pajola et al. (2017), where images of an outburst source region on comet 67P were compared, leading to the conclusion that this specific event has been caused by a cliff collapse. Further numerical simulations of dusty material demonstrated that avalanches could generate a transient, tightly focused outburst plume closely resembling the observed morphology of outbursts emanating from the surface of 67P (Steckloff & Melosh 2016). However, this mechanism predicts that such outbursts should not be directly associated with any increase in gas production (Steckloff & Melosh 2016).

A comprehensive study of outbursts on 67P was carried out by Vincent et al. (2016a). They analysed optical images recorded by the *Rosetta* cameras for a 3-month period around 67P's perihelion passage in 2015 August and identified 34 different dust outbursts. These outbursts were characterized by sudden brightness increases in the coma, lasting only a few minutes, which are distinct from the typically less bright dust jets continuously observed on the rotating comet nucleus (Vincent et al. 2016b). The source locations of the dust outbursts were primarily in the Southern hemisphere, the summer hemisphere at that time, in line with previous observations that show that active sources generally migrate to subsolar regions (Ip et al. 2016; Läuter et al. 2019). They are often found near steep scarps, cliffs, and pits (Rinaldi et al. 2018). Furthermore, Vincent et al. (2016a) observed that outburst events could be classified into two groups, depending on whether they occur at local sunrise or at local noon. Bockelée-Morvan et al. (2017) investigated two outbursts on 67P using infrared data from *Rosetta*/VIRTIS and found evidence of small grains and agglomerates. However, the column densities of H_2O and CO_2 did not change during these events. The authors concluded that these outbursts were likely caused by a cliff collapse similar to the one studied by Pajola et al. (2017).

In this paper, we investigate 45 outbursts on comet 67P observed during various phases of ESA's *Rosetta* mission, with the goal to enhance our understanding of cometary outburst mechanisms. The changes in the gas composition of the comet's coma, as measured with the *Rosetta* Orbiter Spectrometer for Ion and Neutral Analysis (*Rosetta*/ROSINA; Balsiger et al. 2007), are associated with two distinct outburst trigger mechanisms. This nuanced exploration is made possible by the exceptional, continuous monitoring of comet 67P by the *Rosetta*/ROSINA instruments. Section 2 provides details of the ROSINA instruments and data processing procedures, while Section 3 presents the measurements acquired by *Rosetta*. The ensuing discussion in Section 4 brings together our findings and concludes this study.

2 METHODS

2.1 ROSINA/DFMS instrumentation and data treatment

The ROSINA Double Focusing Mass Spectrometer (ROSINA/DFMS) is a double focusing mass spectrometer in Nier–Johnson configuration with a field of view of $20^\circ \times 20^\circ$. Instrument details are given by Balsiger et al. (2007). ROSINA/DFMS contains a toroidally shaped electrostatic analyser, filtering ions for their kinetic energy, and a curved permanent magnet, where the momentum of the ions is filtered. This combination separates different mass-to-charge ratios (m/z) of the incoming ions. The ions are produced by electron impact ionization using a hot filament. The DFMS is a scanning mass spectrometer, where each mass range around an integer m/z is measured sequentially. To do so, a suitable set of voltages is applied to the ion optical system to select a given m/z ratio. In addition, the voltage across the multichannel plate (MCP) detector is adjusted to achieve an appropriately amplified electron current proportional to the incident ion flux. This adjustment creates a gain variation for each measurement and increases the dynamic range of the instrument. The mass resolution is 3000 at the 1 per cent level of the peak for m/z 28 (Balsiger et al. 2007).

After identifying the species in the mass spectrum, a mass scale is applied and the species' signal is integrated (De Keyser et al. 2019). Further, after applying species-dependent sensitivities and fragmentation patterns, the partial densities are obtained after normalization to the total density measured by the ROSINA COmet Pressure Sensor (ROSINA/COPS). More details on DFMS data analysis are given by Le Roy et al. (2015) and Calmonte et al. (2016).

Including the voltage settling time (roughly 10 s per spectrum) and the integration time of the measurement (20 s), a full scan in the typical mass range from m/z 13 to m/z 100 takes about 45 min. In addition, each scan includes two additional m/z 18 measurements, one at the beginning and one at the end of the measurement cycle. This doubling is used to monitor the water activity changes of the comet over the duration of the scan.

2.2 ROSINA/RTOF instrumentation and data treatment

The ROSINA Reflectron-type Time-Of-Flight (ROSINA/RTOF) is the second mass spectrometer of the ROSINA experiment (Scherer et al. 2006). It is designed to measure cometary neutral gas and ions

with a wide and instantaneous mass range (from 1 *m/z* to > 300 *m/z*) and high temporal resolution.

Charged particles are extracted from the ionization chamber towards the drift tube by an extraction grid, applying a pull pulse at a frequency of 2, 5, or 10 kHz. The ions pass through the drift tube, are reflected in the reflectron, pass again through the drift tube and finally reach the detector. The time of flight of each molecule is proportional to the square root of the mass-per-charge of the species.

The first step of the data analysis is to apply the corresponding mass scale to all spectra (Gasc et al. 2017). The second step is integrating the peaks corresponding to the species of interest. The integration yields the numerical area below the curve, which represents the number of ions per 200 or 400 s integration time depending on the operating mode. Having obtained the number of ions per species, corrections due to sensitivity and fragmentation pattern of each molecule were applied as detailed in Gasc et al. (2017). Finally, after normalization to the measured total densities by ROSINA/COPS, the corresponding partial densities of the observed molecules are retrieved. More details of the data analysis applied to ROSINA/RTOF are given in Gasc et al. (2017).

2.3 ROSINA/COPS instrumentation and data treatment

The Comet Pressure Sensor (COPS) completed the ROSINA instrument package (Balsiger et al. 2007). It was designed to measure the gas density in the coma and consisted of two different gauges. In the nude gauge, molecules were first ionized via electron impact, and then the current was measured with an electrometer after acceleration. This gauge measured the total neutral particle density in the coma. The ion current relative to the electron current is related to the density of the neutral gas inside the NG after application of the laboratory-derived calibration factors (Graf et al. 2004; Tzou 2017). The simplicity of the sensor makes it a reliable and stable monitor for the gas density of the comet in the vicinity of the spacecraft. The second gauge, the ram gauge, thermalized the neutral gas molecules first before ionization. Hence, it measured the ram pressure, which is equivalent to the cometary gas flux.

2.4 Data selection and analysis

The outbursts identified by Vincent et al. (2016a) were described as transient jets that were present in a given image, but not in the preceding and following images. Images were taken with a 5 to 30 min cadence, setting a limited timing precision. The lifetime of the dust outburst is minutes up to a few tens of minutes. Knowing the source locations of the dust outbursts, the gas composition in the coma around such events has been studied temporally and spatially. We analysed ROSINA/DFMS data, acquired during the 2015 July–September time period described by Vincent et al. (2016a) and the periods around the outbursts listed in Table 1. In addition, we investigated ROSINA/RTOF data for the 2016 February 19 event, reported by Grün et al. (2016).

To examine the outburst events using ROSINA data, it was necessary to determine the specific instances when the *Rosetta* spacecraft was positioned above a source location corresponding to any of the outbursts. To do so, an angular window of ± 25° in subspacecraft longitude and latitude with respect to the source location was selected. This angular window takes into account the lateral expansion of the gas (e.g. Combi et al. 2012) and the initial, non-radial outflow direction, the duration of a measurement cycle of DFMS, as well as the instrument's spatial resolution for determining the surface distribution of the emission (Marschall et al. 2020b). However, it does not take into account the highly non-spherical morphology of the nucleus. Mitigating this limitation, and accounting for varying spacecraft-nucleus distances, the data set was subjected to normalization. This process, underpinned by the individual spacecraft-event source distance for each measurement instance, effectively rectified the diverse viewing geometries. Given the spatial proximity of several outbursts, a careful evaluation of each data set and its associated measurement configuration was indispensable to be able to link the ROSINA data to distinct events in the images.

Table 1. Summary of all published outburst events on 67P not included in the summer fireworks (Vincent et al. 2016a). For events detected with ROSINA/DFMS the maximum density enhancements for CO_2 and CO relative to H_2O are given. Most of these events were H_2O dominated and thus, density enhancements <1 mean that H_2O was the most dominant driver for the considered event and the enhancement of H_2O would be the inverse of the given value. Uncertainties on the enhancements are ±18 per cent, mostly due to instrument calibration uncertainties (Le Roy et al. 2015; Calmonte et al. 2016).

Event Date	Region	ROSINA Detection	Enhancement CO_2	Enhancement CO
2014 Apr[1]	Not given[d]	Too far	–	–
2015 Mar 12[2]	Imhotep[c]	Inst. off	–	–
2015 May 23[3]	Not given[d]	Yes	0.2	0.2
2015 July 10[4]	Aswan[a]	Inst. off	–	–
2015 Aug 10[5]	Khonsu[d]	Inst. off	–	–
2015 Sept 03[6]	Not given[d]	No loc.	–	–
2015 Sept 13[5,7]	Imhotep[d]	Yes	0.9	0.5
2015 Sept 14[5,7]	Atum[d]	Yes	0.9	0.4
2015 Sept 23–30[6]	Not given[d]	No loc.	–	–
2015 Nov 07[8]	Southern neck[b]	Yes	8.4	1.2
2016 Jan 06[9]	Imhotep[a]	Yes	0.6	0.3
2016 Feb 19[10]	Atum[a]	Yes	0.5	0.2
2016 July 03[9]	Imhotep[a]	Yes	0.5	0.7

Notes. References: (1) Tubiana et al. (2015); (2) Knollenberg et al. (2016); (3) Feldman et al. (2016); (4) Pajola et al. (2017); (5) Rinaldi et al. (2018); (6) Lin et al. (2017); (7) Bockelée-Morvan et al. (2017); (8) Noonan et al. (2021) (Event B); (9) Agarwal et al. (2017); (10) Grün et al. (2016).
Local time of event: (a) sunrise; (b) midday; (c) night; (d) unknown.

It is important to consider the temporal offset between remote sensing (e.g. *Rosetta* cameras) and *in situ* observations (e.g. ROSINA instrument) of the same event. *In situ* measurements require gas to flow into the instrument, while cameras are most sensitive to illuminated dust outbursts from a phase angle of 90°. Additionally, the outflowing gas from the outbursts is much faster (≈ 0.5–0.9 km s^{-1}; Biver et al. 2019) than the dust grains (≈ 22–65 m s^{-1}; Rinaldi et al. 2018). We took these various effects into consideration in the analysis of the ROSINA data. Additionally, it is clear that the gas flow smears out inhomogeneities in surface production from small-scale source regions (a few metres to a few tens of metres) when the gas is measured at a distance. During 2015 July to September, the spacecraft was far away from the comet's surface (>180 km). Hence, it is not possible to exactly localize the source of the gas density enhancements recursively observed over several nucleus rotations with the ROSINA instruments. Nevertheless, the measured gas density enhancements are an indicator for the general outgassing behaviour of the source regions and their surrounding areas.

For this analysis, the densities of different volatiles are compared to H_2O. Fig. A3 shows how to retrieve the data used. To calculate the enhancement each time *Rosetta* was above the source location, the peak density of both CO_2 and H_2O has been selected and corrected

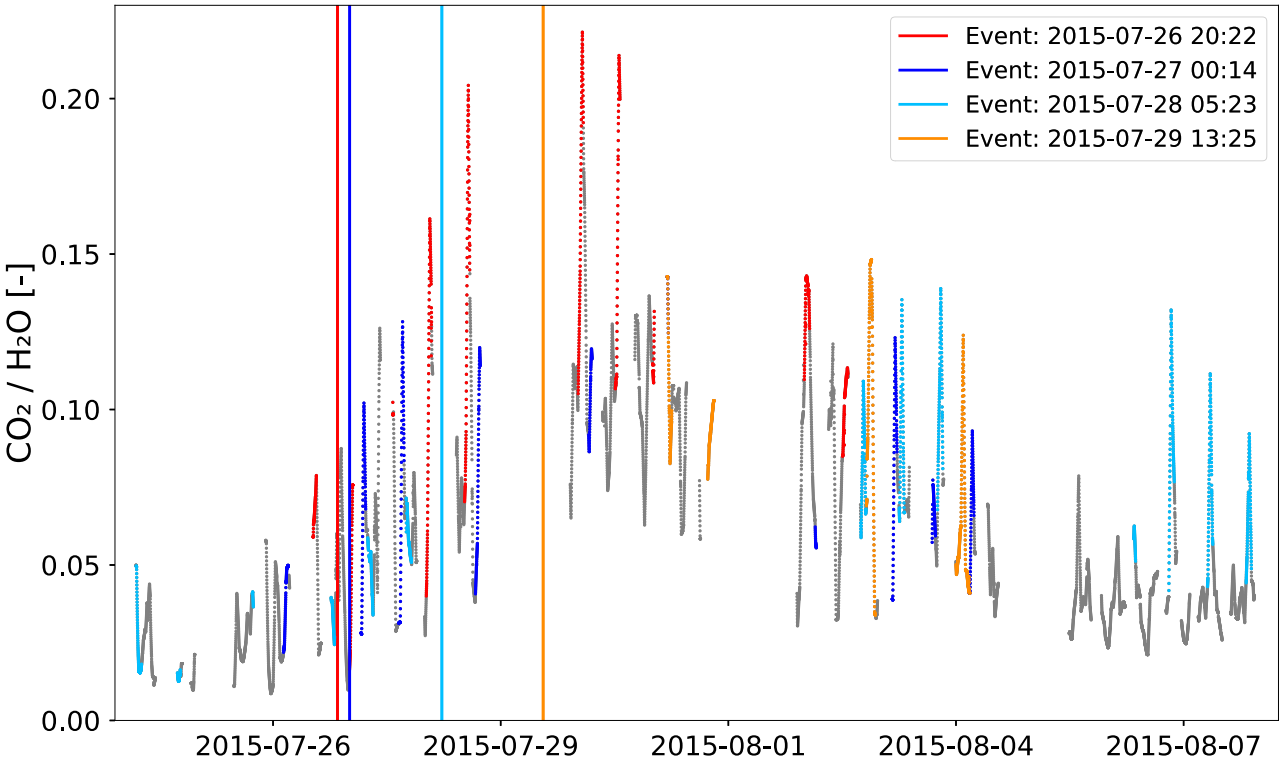

Figure 1. Ion count ratio from ROSINA/DFMS for CO_2 relative to H_2O from 2015 July 24 until August 8. The coloured data points show measurements taken when the *Rosetta* spacecraft was flying over the identified source location of the respective event observed by the *Rosetta* cameras at the time marked by the corresponding vertical line. For a better representation, only a part of the summer fireworks' period (Vincent et al. 2016a) and only four distinct events are shown. The first three events were morning outburst whereas the last event (orange) was a midday outburst.

considering the quiescent coma. It is possible that the peak values are slightly shifted in time due to the mass scanning nature of the instrument. These time shifts, on the order of a few minutes, do not affect the enhancement calculations as the time-scales associated to *Rosetta* passing above the active region is substantially longer. Finally, the relative density enhancement for the volatile species x is then calculated by:

$$e_x = \frac{(n_x/n_{H_2O})_{peak}}{(n_x/n_{H_2O})_{qs}} = \frac{(c_x/c_{H_2O})_{peak}}{(c_x/c_{H_2O})_{qs}} \quad (1)$$

with n the density and c the DFMS detector signal where fragment contributions have been removed (Rubin et al. 2019).

The density enhancement, e_x, shows how much the ratio at the peak, within the aforementioned subspacecraft longitude and latitude window (denoted as *peak*), is increased at that time compared to the quiescent coma ratio (denoted by *qs*). Consequently, it shows the increased release of a volatile species during an outburst event as compared to the nominal comet outgassing. The quiescent coma is retrieved from measurements at the same activity levels of the comet and similar *Rosetta* positions as the source location of the dust outburst (see Extended Data Fig. A3). A caveat to using this definition of the relative enhancement calculation exploiting two ratios is that an enhancement increase might also occur if there was a decrease in just the H_2O density. However, as background corrections are applied to equation (1), a decrease of H_2O would imply a negative ratio, which has not been observed for any of the events analysed. All of the events showed behaviours similar to what is depicted in Figs 2 and A3.

3 RESULTS

3.1 Summer fireworks

The 34 so-called summer fireworks outbursts during the summer of 2015 (from 2015 July 10 to September 26), studied by Vincent et al. (2016a), represent the largest sample of examined outbursts to date. While the dust features associated with these outbursts have been thoroughly analysed (Vincent et al. 2016a), little is known about their gas component. Thus, we investigated gas abundance ratios for the most abundant highly volatile species detected in comet 67P's coma (Rubin et al. 2019) relative to H_2O using data from *Rosetta*/ROSINA.

Fig. 1 depicts the CO_2 signal compared to H_2O measured with ROSINA/DFMS from 2015 July 24 to August 8 to show how the changes in this ratio are attributable to fly-overs of the *Rosetta* spacecraft over the corresponding outburst event source regions. For a better representation, only this part of the complete summer fireworks period is shown together with a selection of three distinct events. For the full time period, we refer to Extended Data Figs A1 and A2. CO_2 is the second most abundant gas after H_2O (Hoang et al. 2019; Läuter et al. 2019; Rubin et al. 2019). In the following, gas ratios relative to H_2O will be discussed and thus only the gas in the numerator will be mentioned to simplify the nomenclature.

The typical signature of the outbursts during the summer fireworks period, when the spacecraft was positioned above one of the source regions (Vincent et al. 2016a), was an increase in the relative abundance of highly volatile species (i.e. species with sublimation temperatures below that of water), especially CO_2, which later returned to pre-outburst levels. In contrast, H_2O showed only marginal increases (Fig. 2). As a result, the activity of highly volatile species

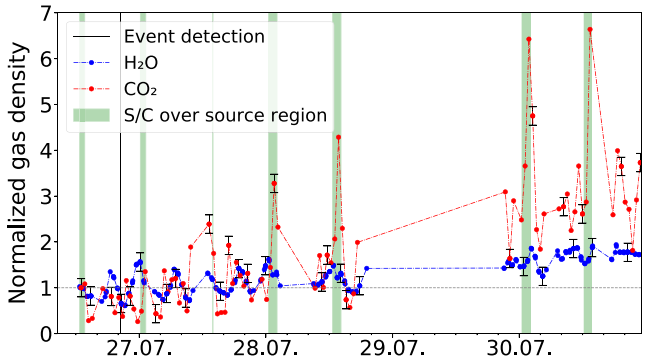

Figure 2. Gas densities of H_2O and CO_2 normalized to their quiescent coma levels during the CO_2 enhanced outburst from 2015 July 26 measured with ROSINA/DFMS. The quiescent values have been retrieved a few hours before the dust event. Uncertainties are only shown on every 10th data point for H_2O and on every 5th data point for the other volatiles to improve visibility. The vertical line represents the time when the event has been detected by the *Rosetta* cameras and the green areas represent the time when the spacecraft was above the considered outburst source region. The grey horizontal line shows the quiescent level of the normalized data. The continuous increase of both H_2O and CO_2 is due to the spacecraft's movement across the generally more active Southern hemisphere of 67P during that time.

gradually increased and typically ceased a few days after the visible outburst.

The enhancement in relative abundance in 67P's coma for each flyover was calculated following the methodology described in Section 2.4 and detailed results are given in Table A1. While the enhancement patterns exhibit similarities across all events, characterized by an increase around the time of the event being detected by the cameras and followed by a decrease a few days later, they differ in terms of the starting time, duration, and magnitude of enhancement. Analysis of the weighted mean enhancement in relative abundance as a function of time with respect to the optical detection of the dust feature of the events reveals that the average enhancement of volatiles already starts up to three days (∼6 rotations) prior to the observed expulsion of dust indicating that the dust component of the outbursts may be preceded by an increase in outgassing of highly volatiles (Fig. 3). Subsequently, the mean density enhancement gradually decays, with a notably slow decrease over a period of up to 8 d (∼16 rotations) compared to the short-lived nature of the ejected dust during the event observed by the cameras. Hence, only the combined analysis of dust and gas can give a comprehensive view of the nature of the outbursts and their trigger mechanisms. The average enhancement is weighted with the weight for each individual point being inversely proportional to its statistical uncertainty, so that events where *Rosetta* was closer to the source region and the data are less smeared out are given a higher weight than events measured from a larger distance with less signal and more measurement uncertainties. The considered data set has been thoroughly analysed and most of the individual outbursts were well separable. None the less, it is possible that different events may overlap, increasing the mean density enhancement, especially at times long before and long after the observed dust outbursts. In addition, events not observed by the *Rosetta* cameras might also contribute to the mean density enhancement over time.

Fig. 4 illustrates the average density enhancement relative to water for the most abundant species detected in comet 67P's coma (Rubin et al. 2019) during the summer 2015 events. The mean enhancement for the sunrise and midday events, as well as the mean enhancement over all summer 2015 events, are presented separately. When considering all events combined, CO_2, ethane (C_2H_6), and propane (C_3H_8) exhibit higher enhancements (approximately ×13) compared to carbon monoxide (CO), hydrogen sulphide (H_2S), ammonia (NH_3), methane (CH_4), formaldehyde (H_2CO), methanol (CH_3OH), and hydrogen cyanide (HCN) (×3 to ×6). These findings align with Rubin et al. (2023), where C_2H_6 and C_3H_8 are primarily associated with CO_2, while CO, H_2S, NH_3, CH_4, H_2CO, CH_3OH, and HCN are distributed in roughly equal proportions between water and CO_2. Consequently, the enhancement of the latter molecules is reduced to the fraction associated to CO_2. This results in their enhancement being smaller than that of CO_2 and its associated molecules, but larger than that of water and its associated molecules. Additionally, it appears plausible that part of the signal from molecules, such as to NH_3, originates from semivolatile salts on dust grains (Altwegg et al. 2020, 2022), ejected during the outburst. The correlation between O_2 and H_2O is consistent with previous observations (Bieler et al. 2015; Rubin et al. 2023). Consequently, these results suggest that CO_2, as the most abundant highly volatile species, plays a pivotal role in driving outburst events and carries a suite of associated species along.

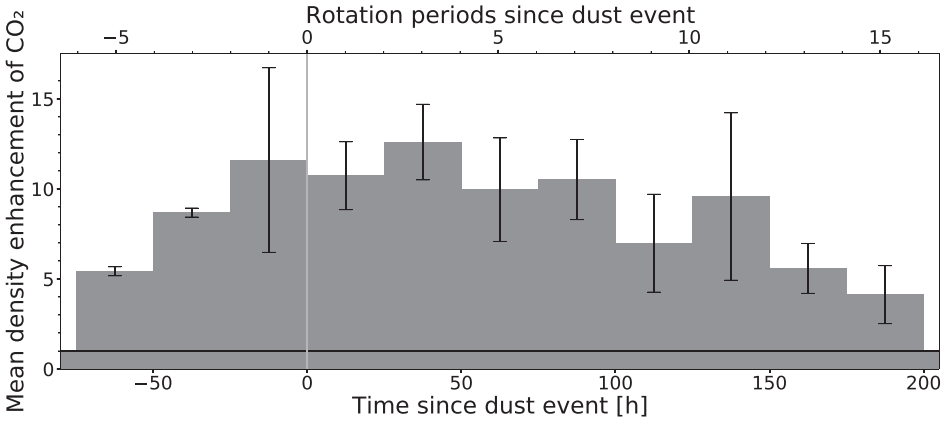

Figure 3. Weighted mean density enhancement for CO_2 during the summer fireworks outburst events as a function of time. The enhancement is the maximum of the ratio CO_2/H_2O during each fly-over divided by the same ratio in the quiescent coma. Time zero represents the time when the dust event has been observed with the *Rosetta* cameras (timing precision is 5 to 10 min). The horizontal line shows the unchanged ratio (enhancement factor of 1). Only events exhibiting a CO_2 enhancement are considered.

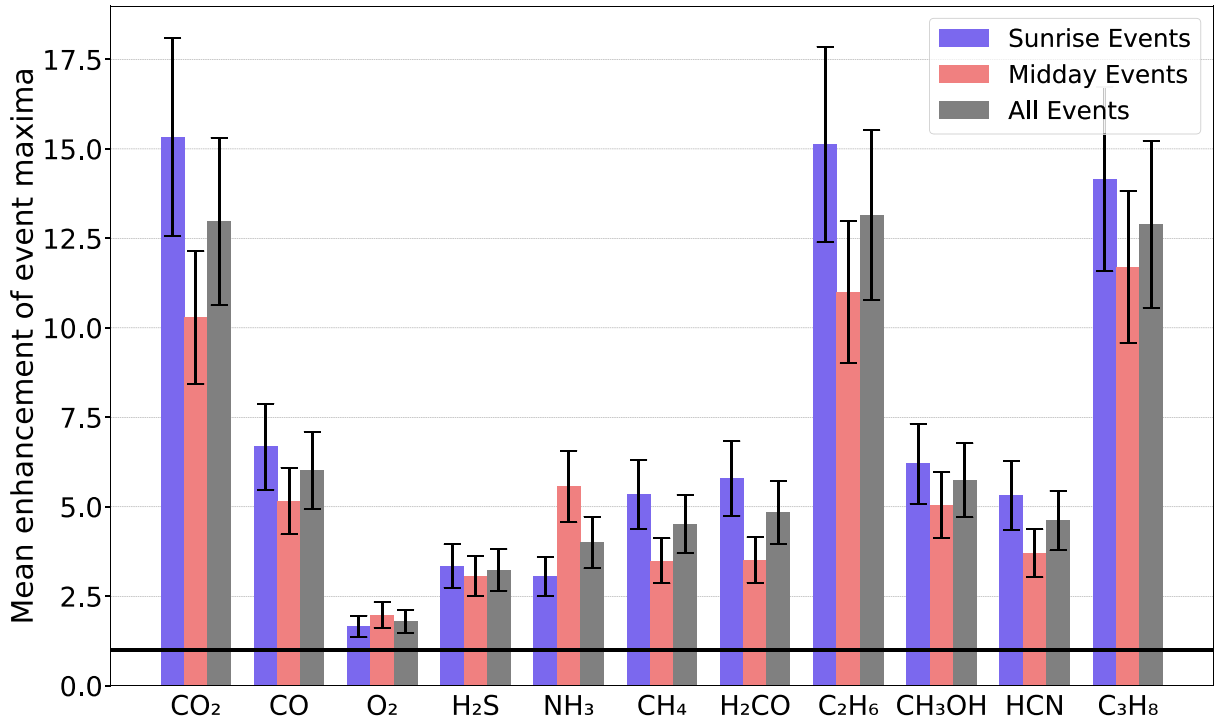

Figure 4. Weighted mean values of maximum density enhancement separated for sunrise and midday events and all events combined for the summer fireworks 2015 period reported by Vincent et al. (2016a). The uncertainties show the standard deviation of the mean including uncertainties of the individual measurements as explained in Section 2 as well as the variation of H_2O for each considered event. The black horizontal line shows the unchanged ratio (enhancement factor of 1). The volatiles are sorted by their relative bulk abundance compared to H_2O (Rubin et al. 2019).

In agreement with Vincent et al. (2016a), our analysis supports the categorization of summer firework events into two groups: sunrise and midday events, determined by the local time of the outburst source regions. On average, with the exception of NH_3, sunrise events exhibit slightly higher density enhancements compared to midday events (Fig. 4). However, the error bars overlap and uncertainties persist due to the limited temporal coverage of the outburst events. Thus, clear differentiation between these groups is not possible as also no correlation exists between the outburst type and its local time (Vincent et al. 2016a). None the less, Vincent et al. (2016a) suggested that the two groups might be associated with different mechanisms. Noon outbursts may be linked to buried pockets of volatiles, which require time to get heated enough to trigger an outburst. Shortly after noon is when the local (sub)-surface reaches its maximum temperature. On the other hand, early morning outbursts occur almost immediately as the Sun rises. Despite the temperature possibly not being very high, the very low thermal inertia ensures that these local times exhibit the steepest temperature gradient. The surface heats up rapidly, with the gradient being large enough to trigger thermal cracking, potentially leading to surface breakage. This rapid heating might explain the slightly higher volatile enhancements for the sunrise events, as the immediate surface breakage might release gas more intensively. For slowly heated pockets, the confined gas might already start to seep out more gradually before the abrupt ejection of dust occurs. However, this is only a suggestion and the data are not sufficiently different to make a definitive statement. An explanation on why NH_3 exhibits a converse enhancement for the two groups might be that NH_3 comes from ammonium salts that might take some time and need high temperature to sublimate or build up which is possible for the midday events.

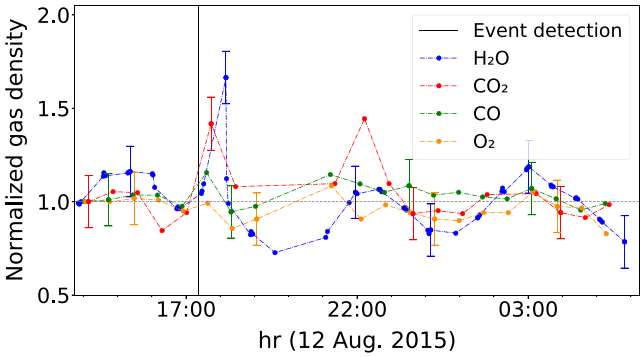

Figure 5. Gas densities of H_2O, CO_2, CO, and O_2 normalized to their quiescent coma levels during the water enhanced outburst 2015 August 12 measured with ROSINA/DFMS. The quiescent values have been retrieved a few hours before the dust event. Uncertainties are only shown on every 10th data point for H_2O and on every 5th data point for the other volatiles to improve visibility. The vertical line represents the time when the event has been detected by the *Rosetta* cameras. The grey horizontal line shows the quiescent level of the normalized data.

As anticipated, not all summer firework events exhibited an enhancement of highly volatile species. Some events displayed no volatile enhancement or even an increase in the water signal. For instance, the event on 2015 August 12 (#14 in Vincent et al. 2016a), resulted in a twofold increase of H_2O compared to CO_2 and an increase of a factor 5 of water compared to CO (Fig. 5). This event has a source region with a morphology expected from the modelling of cliff collapses. Hence, considering the water enhancement, this event might have been triggered by a cliff collapse. Another event hinting

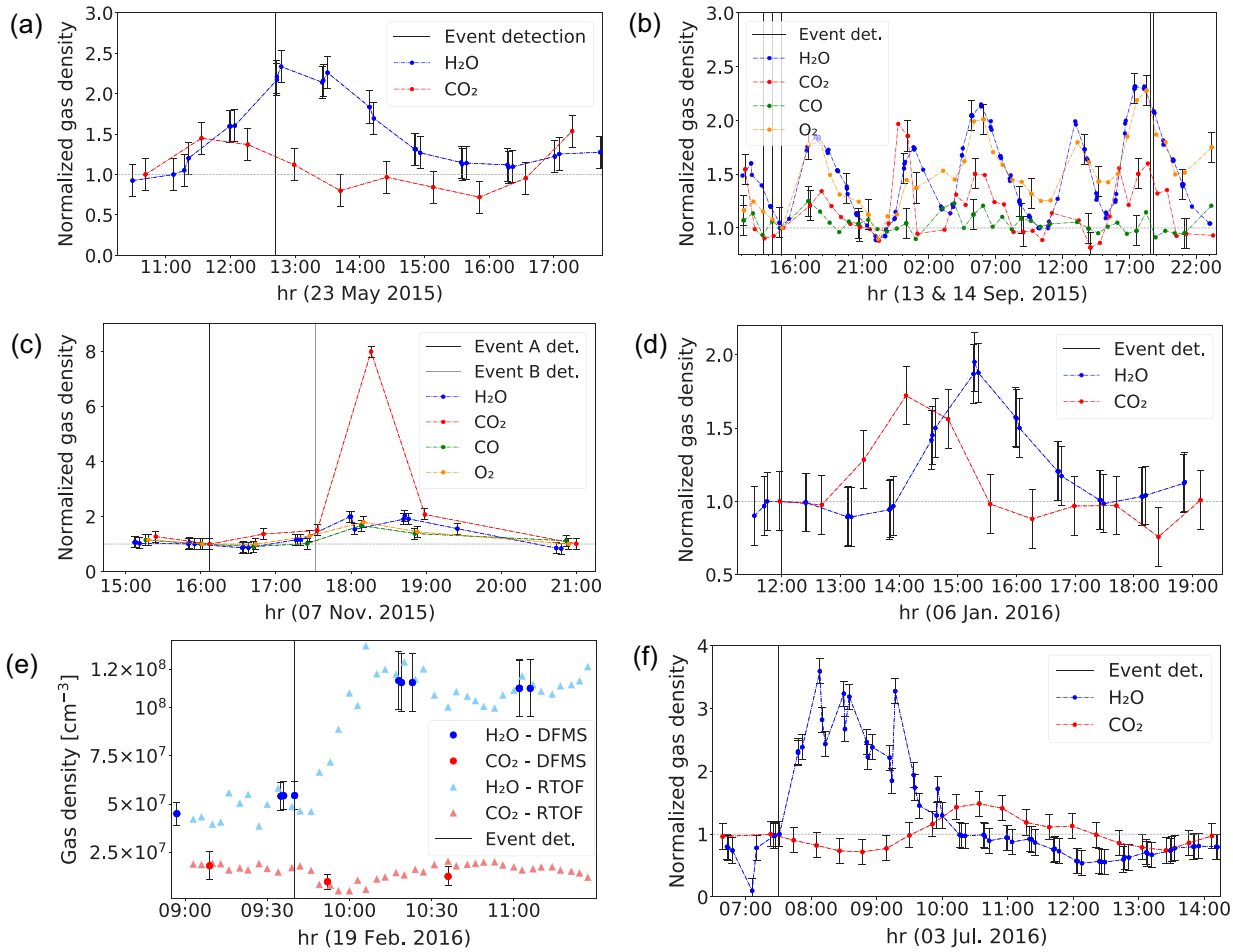

Figure 6. Gas densities of H_2O and CO_2 normalized to their quiescent coma levels during the outbursts of (a) 2015 May 23, (b) 2015 September 13 and 14, (c) 2015 November 7, (d) 2016 January 6, and (f) 2016 July 3 measured with ROSINA/DFMS. Panel (e) represents the absolute gas densities of H_2O and CO_2 for the outburst observed on 2016 February 19 measured with both the ROSINA/DFMS and the ROSINA/RTOF. The absolute densities are displayed in panel (e) to underline that both instruments acquired the same absolute results and no normalization or instrument effect occurred. Error bars show uncertainties of the DFMS measurements. In panel (b), uncertainties are only displayed on every 15th data point for H_2O and on every 5th data point for the other volatiles to improve readability. RTOF uncertainties are not shown because they are of the order of the symbols. The vertical lines represent the times when the dust events have initially been detected by the *Rosetta* cameras (the dust events could have started up to 5 to 30 min before). The grey horizontal lines show the quiescent level of the normalized data.

at a cliff collapse was on 2015 September 14 (#33 in Vincent et al. 2016a), showing a 15 per cent increase in water density compared to CO_2 and a twofold increase compared to CO (Fig. 6b). This event has already been investigated with the *Rosetta* Visible InfraRed Thermal Imaging Spectrometer (VIRTIS) (Bockelée-Morvan et al. 2017) where the authors stated that no large increase of H_2O and CO_2 has been measured but very small grains or agglomerates should be present. They suggested an excess signal of organic species and hydrocarbons where our results show an increase of CH_3OH by about 50 per cent, aligning with their results. Unfortunately, ROSINA measurements are unavailable for the event on 2015 July 10 (#1 in Vincent et al. 2016a), described as an additional cliff collapse event by Pajola et al. (2017). Thus, while most summer fireworks events showed enhancements in highly volatile species, particularly CO_2, cliff collapse events also occurred during this period, marked by slight increases in the water signal.

The spacecraft trajectory determined when the ROSINA instruments were able to measure above an outburst source region. Hence, illumination or local time during the observation are purely defined by the spacecraft trajectory and no conclusion can be drawn from whether or not the measurements were taken above an illuminated surface. However, ROSINA measures the gas cloud ejected during the event after its travel and dispersion, so that the conditions at the time of the observations only depend on the conditions at the time of the dust event and on the dynamics of the gas cloud, not on the instantaneous conditions at the time of the observation. The spacecraft was mostly on a terminator orbit with a phase angle of 90°. Consequently, although the spacecraft's position and viewing geometry do not permit a measurement of the immediate outburst gas and a smear-out of inhomogeneities due to the large distance of the spacecraft to the comet's surface is expected, ROSINA is still able to investigate the composition of the outgassing of the source regions and their surrounding areas both before, during, and after the dust event.

3.2 Other outbursts

Besides the outbursts described in Vincent et al. (2016a), a few other outburst events have been detected on 67P during the *Rosetta* mission. Table 1 provides a list of these events, including their

estimated source location on the nucleus, and whether or not they were detected by the ROSINA instruments. The first reported event (Tubiana et al. 2015) occurred when the *Rosetta* spacecraft was too far from the comet for ROSINA to detect volatile signals above the spacecraft background (Schläppi et al. 2010), and during the second event (Knollenberg et al. 2016), the ROSINA instruments were not operating.

Feldman et al. (2016) examined outbursts occurring between 2015 May and July using the Alice far-UV spectrograph. These events were unrelated to the summer fireworks and were not detected in the visible wavelength range captured by the other *Rosetta* cameras. Unfortunately, *Rosetta* was mostly above the less active Northern hemisphere and the outburst source locations for these events remain unknown. Nevertheless, the event on 2015 May 23 showed peaks in the relative abundance of different volatiles detected by DFMS (Fig. 6a), with a rapid increase in H_2O observed just 8 min after detection by Alice (Feldman et al. 2016). The enhancement of H_2O relative to CO_2 and CO was $\times 10$ and $\times 4.5$, respectively. The O_2 levels also increased together with H_2O. Considerable amounts of H_2O and notably high densities of O_2 compared to the quiescent level were also reported by Feldman et al. (2016), indicating that the event on 2015 May 23 was driven by H_2O sublimation.

The events on 2015 July 10 and 2015 August 10, as described in Pajola et al. (2017) and Rinaldi et al. (2018), respectively, were not observed because DFMS was not operated during that period. Outbursts on 2015 September 13 and 14 were observed by VIRTIS (Bockelée-Morvan et al. 2017; Rinaldi et al. 2018). The researchers concluded that the outburst measurements could be attributed to the presence of very small ice particles. While the CO signal measured with DFMS remained relatively constant, the signatures of H_2O, CO_2, and O_2 increased slightly. There was no significant enhancement of H_2O relative to CO_2, with only a twofold increase in H_2O relative to CO (Fig. 6b). O_2 closely followed the H_2O signal, as explained by the association of these two molecules (Rubin et al. 2023).

Lin et al. (2017) studied additional outbursts during the summer fireworks phase, alongside those in Vincent et al. (2016a). Unfortunately, the source locations of these outbursts remain unknown and the mass spectrometers of ROSINA were inactive from 2015 September 23 to 30 due to large cometary distances, missing a substantial portion of these events.

Noonan et al. (2021) investigated two outbursts (A and B) occurring on 2015 November 7 (A: 16:07 UTC, B: 17:32 UTC), and determined their source locations. The gas composition during the events was captured by DFMS measurements (Fig. 6c). Outburst A did not show significant signal changes. However, outburst B exhibited a notable increase in CO_2 with only a marginal increase in H_2O. No DFMS data were available after 19:30 UTC. The gas enhancement ratio of approximately $\times 8$ for CO_2 to H_2O aligns with the findings of the summer 2015 outbursts and supports the highly volatile-dominated nature of outburst B as proposed by Noonan et al. (2021).

A well-documented outburst took place on 2016 February 19, and was extensively observed by multiple *Rosetta* instruments (Grün et al. 2016). The source of the outburst was identified in the Atum region, near a steep cliff, where thermal stress, fracture mechanics, and gravity possibly triggered a landslide, exposing fresh ice to direct sunlight and triggering the release of gas and dust. Both ROSINA/RTOF and ROSINA/DFMS instruments were operated during that time and observed a notable increase in H_2O accompanied by a more or less stable CO_2 signal (Fig. 6e), indicating a water-driven outburst with a density enhancement of $\times 2$ for water compared to CO_2. The H_2O signal rapidly increased and remained high during the analysed time period, which aligns with observations by the MIRO instrument of the gas surrounding *Rosetta* (Grün et al. 2016).

On 2016 July 3, a distinct outburst took place in the Imhotep region's circular Basin F, which was observed by multiple *Rosetta* instruments (Agarwal et al. 2017). The outburst occurred during local sunrise and resulted in the formation of a 10-metre-sized dust-free icy patch on the surface. Data from ROSINA/DFMS revealed a significant increase in H_2O following the event, with short spikes reaching up to 3.5 times the quiescent level (Fig. 6f). Including a time shift due to different velocities of the gas and the dust, this is consistent with the GIADA data (Agarwal et al. 2017). The density enhancements of water relative to CO_2 and CO were $\times 2.2$ and $\times 1.5$, respectively.

Additionally, a smaller but similar dust plume was observed by Agarwal et al. (2017) on 2016 January 6, near the source region of the 2016 July event, shortly after the local sunrise, suggesting the south-western walls of the circular depressions in the Imhotep Basin F as preferred location for morning outbursts. The DFMS data showed that the H_2O density increased more than the CO_2 by a factor of 1.6 with a shift in time of about one hour, suggesting a water-driven event (Fig. 6d). The analysis of both outbursts was limited to a short-term analysis due to limited coverage.

The analysis of published outburst events reveals a clear distinction between water-dominated and CO_2-dominated events. Most of the events, excluding the summer 2015 period, were primarily driven by water (Table 1). Notably, the event B (Noonan et al. 2021) on 2015 November 7 stands out as a CO_2-dominated outburst occurring outside the summer 2015 period. The distinct driving mechanisms may be associated with different conditions at the source regions. Water-dominated events mostly occurred outside the most active surface areas in terms of surface emission rates (Läuter et al. 2019) or below cliffs, while the CO_2-dominated event on 2015 November 7 occurred in a source region with multiple documented events (Vincent et al. 2016a). These findings highlight the diversity and complexity of outburst dynamics.

4 DISCUSSION

The ROSINA study of 45 outbursts on 67P shows two distinct groups of events: water-driven and CO_2-driven outbursts. These groups also exhibit a different temporal evolution. The water-driven events showed rapid changes in the coma composition, enhancing the density of H_2O more than that of other coma constituents for only a few hours. In contrast, the CO_2-driven group of events (summer fireworks and event B of 2015 November 7) displayed a slow increase even before the event was observed by the *Rosetta* cameras in the form of a bright dust jet lasting only a few minutes, and an even slower subsequent decrease of CO_2 compared to H_2O in the coma above the source region, lasting for several days. Thus, the coma composition at the distance of *Rosetta* changes much more slowly than the observed dust ejection for the same events.

We find that several highly volatile species such as CO_2, CO, and alkanes have been largely enhanced during the CO_2-driven gas outbursts. CO_2 being the most abundant molecule after H_2O (Rubin et al. 2019), its enhancement during these events is most significant. The clear distinction in coma composition during the outbursts as well as their different temporal behaviour leads to the conclusion that these groups of events are triggered by two different mechanisms.

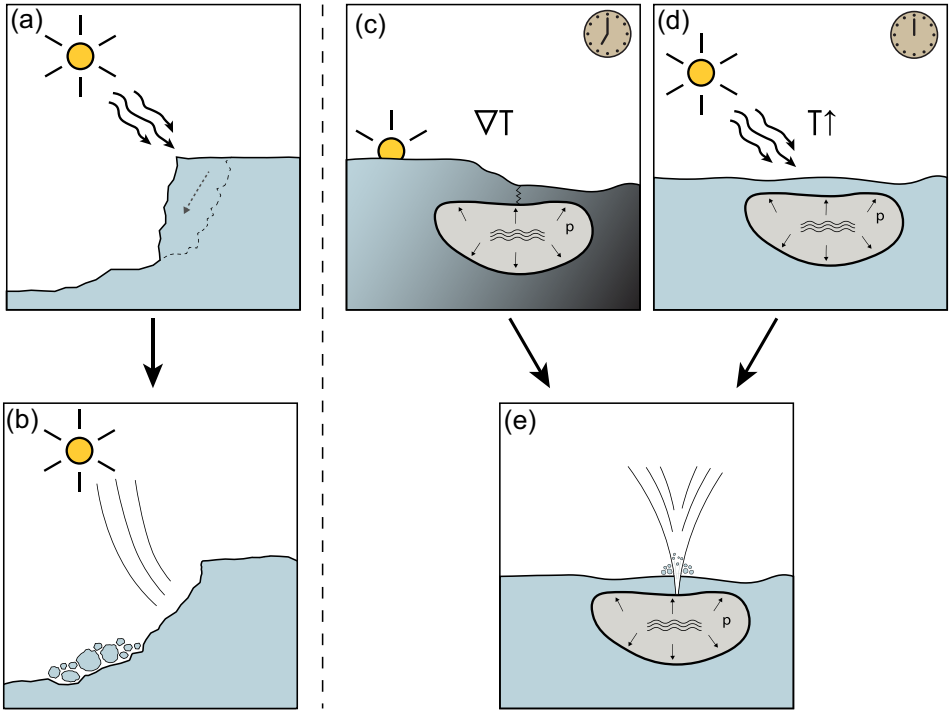

Figure 7. Schematics of outburst trigger mechanisms: (1) Cliff collapse: (a) Solar illumination heats up a cliff that collapses due to thermal formation of small cracks. The collapse releases dust from the surface seen as an outburst in the visible range of the cameras. (b) After the collapse, freshly exposed water ice sublimates and the released gas can be measured by the *Rosetta* instruments. (2) Gas pockets: (c) A large temperature gradient due to the local sunrise induces cracks where subsurface pressure pockets containing volatiles can release their pressurized gas leading to an outburst. (d) The high temperature at local noon heats up the surface and subsurface. This increases the pressure in the gas pockets until the pressure is high enough to overcome the tensile strength of the surface inducing an outburst. (e) When the surface cracks are large enough or the pressure has been increased enough as shown in (c) and (d), the pressurized gas pockets violently release dust and gas. Panels (c)–(e) only show the triggering mechanism of the event and do not display the continuous outgassing before and after the CO_2-driven outbursts.

Earlier studies proposed three main outburst trigger mechanisms:

(i) High-pressure pockets of highly volatile species below the surface layers (e.g. Belton et al. 2013; Agarwal et al. 2017; Bockelée-Morvan et al. 2022).
(ii) Collapse of cliffs (e.g. Vincent et al. 2016a; Pajola et al. 2017).
(iii) Amorphous-to-crystalline phase transition of water (e.g. Agarwal et al. 2017).

Agarwal et al. (2017) proposed that the transition of water from amorphous to crystalline ice might induce a sublimation rate similar to the measured dust production rate. This would only be true for pure water ice. However, pure water ice is neither observed in interstellar clouds, nor on the ice mantles on interstellar dust grains, which are believed to be the source of the ices in cometary nuclei. Interstellar water ices contain substantial amounts of impurities including CO_2, CO, and CH_4 (e.g. Crovisier 1999; Boogert, Gerakines & Whittet 2015). In a non-pure water ice mixture with more than 2 per cent impurities, as expected for a comet, the transition from amorphous to crystalline ice has been demonstrated to be endothermic (Kouchi & Sirono 2001). These authors also state that an endothermic crystallization suppresses outbursts.

Contrarily, Prialnik & Jewitt (2022) propose that a burst of crystallization could be initiated by a heat wave propagating from the insolated comet surface to the crystalline–amorphous ice boundary, provided it carries sufficient energy to raise the local temperature to the crystallization point. Once this occurs and the boundary has moved deeper into the nucleus, later heat waves from the surface are too weak to rekindle crystallization when reaching the boundary, leading to a quiescent period. Sublimation then causes the surface to recede from the crystalline–amorphous ice boundary until a new burst of crystallization occurs. This, in turn, affects the time span to the next spurt of crystallization. Hence, this process is particularly relevant for new comets with amorphous ice close to the surface, active beyond the distance where ice sublimation controls cometary activity, as observed in comets C/2003 A2 (Gleason) by Meech et al. (2009) or C/2017 K2 (PANSTARRS) by Jewitt et al. (2017) at 11.5 and 23 au, respectively. Another possible scenario is that crystallization and gas confinement occur together, leading to an outburst (Samarasinha 2001). Despite several observations, simulations, and laboratory studies of cometary outbursts, Prialnik & Jewitt (2022) note that direct evidence for the role of amorphous ice in comets remains elusive due to its nature and burial below the surface in evolved comets like 67P. Consequently more laboratory work to determine the thermophysical properties of amorphous and crystalline ices, especially when loaded with other volatiles, is needed to confirm if the transition from amorphous to crystalline water ice remains a plausible outburst trigger mechanism.

Alternatively, pockets of volatiles below the devolatilized surface layer might build up pressure until they overcome the tensile strength of the surface above and cracks start to appear in the surface layer. The cracks might be formed by a large temperature gradient due to the local sunrise combined with the small thermal inertia of the comet's surface (Fig. 7c). Another possibility is that the cracks slowly progress until the pressure in the gas pockets is high enough (due to the high noon temperature; Fig. 7d) for a bursting to occur. All the gas is released and drags along some of the surrounding

non-volatile material (Fig. 7e). Notably, both of these processes are not on/off processes, i.e. gas may be seeping out from smaller cracks already before the big outburst, which is consistent with the findings of our analysis, as a slow increase in highly volatile species has been measured already before the dust ejection occurred. This combined process can be understood similarly to a pressure cooker where some steam gets released through the safety valve before the pressure increases too much. At a certain pressure, the small seeping cracks cannot release enough gas to maintain the pressure below the pocket's tensile strength and an explosive event occurs, which is what *Rosetta*'s cameras registered as the dust feature of the outburst. If the thermophysical properties of amorphous and crystalline ices support the theory that their transition might trigger outburst events, it would also be plausible that this effect could be responsible for the cracks initiating the bursting of gas pockets. It is prudent to note, that the CO_2-dominated events occurred around generally more active areas on the comet nucleus. Hence, the increase long before the outburst has been observed by the cameras, and long after it ceased (Fig. 3), might also be supported by a generally more active source region. Additionally, the bursting of a pressure pocket not only releases the confined gas but also exposes areas of fresh ice that sublimates and hence increases the densities of H_2O as well as of the volatiles associated with the water ice (Rubin et al. 2023) for a longer time than the dust outburst observed with the cameras, leading to a prolonged enhancement of CO_2 and other highly volatile species.

To have gas pockets, where a significant gas pressure builds up, the porous structure of the comet interior has to be sealed. A possible mechanism could be refreezing of CO_2. It is known that for 67P, CO_2 sublimates long after water stops sublimating on the outbound leg of the comet's orbit (Läuter et al. 2019) from areas, which by then are no longer exposed to sunlight. Such an extended orbital frost cycle of CO_2 has been proposed by Rubin et al. (2023). Due to low gravity, the sublimating gas will be dispersed in all directions, not only upwards, but sideways and downwards. In the interior, it will eventually encounter colder temperatures, where it can refreeze, creating a volatile enriched ice layer (Prialnik & Jewitt 2022). This mechanism may not only explain the extended orbital frost cycle but also presents a potential diurnal day-to-night refreezing process, leading to the creation of gas pockets in regions dominated by highly volatile species over short time-scales.

Laboratory experiments for Martian conditions show that CO_2 is deposited in the form of ice slabs or crystals depending on temperature and pressure (Portyankina et al. 2019). In the experiments, the ice layer conformally coats all the surfaces of the cooling plate, draping even protruding elements. Although the conditions in the comet are different from the laboratory experiments (pressure, temperature, porosity, composition, size), a similar process could happen, where CO_2 covers the porous material with an impermeable layer, which has a considerable tensile strength, enough to confine a gas pocket at elevated pressure (Prialnik & Jewitt 2022). Laboratory experiments show that an ultimate CO_2 ice tensile strength of ∼2–6 MPa is reached (Kaufmann et al. 2020). This strength is in agreement with the suggested ∼2 MPa tensile strength of water ice under Martian conditions used in earlier studies (Mellon 1997). On 67P, once the surface areas come into summer again, a similar effect could take place even though the cometary surface is mostly covered by dust and not transparent as seen on Mars. None the less, CO_2 starts to sublimate from the top building up pressure in the pocket. Eventually the surface layer will crack due to the buildup of the inside pressure and/or due to erosion of the surface layer.

The possibility of gas pockets has already been discussed for comet 9P/Tempel (Belton et al. 2008). The authors concluded that this mechanism will lead to the formation of a small pit or depression and potentially exposes fresh and highly volatile material that will continue to sublime (Belton et al. 2013). A similar result has been discussed for comet 67P in the case of the Imhotep outburst observed in 2015 February (Knollenberg et al. 2016).

The source regions of the summer fireworks are situated near morphological boundaries, clustered into three primary regions displaying irregularities in contrast to the generally flat morphology of the Southern hemisphere. This seems to indicate a link between morphology and outbursts (Vincent et al. 2016a). These source regions are notably rich in CO_2. Nine activity areas, encompassing the most active surface elements contributing to 50 per cent of the total emission, were identified by Läuter et al. (2019), with most summer fireworks sources located in these high-activity areas. The same authors also demonstrated that these areas remain CO_2-rich throughout the mission. This raises the question whether the here described enhancement of highly volatile species might be a result of the overall CO_2-rich outgassing behaviour of the comet's Southern hemisphere.

Läuter et al. (2019) utilized the same ROSINA data set as presented here. However, their results are based on data averaged over specific periods and their results are presented for three intervals with data averaged over 50 d for the data before and after perihelion and even 100 d for data around perihelion. This methodology averages over short-lived events like outbursts, potentially impacting the identification of Southern active sources by Läuter et al. (2019). None the less, the presence of the same CO_2-rich areas long before and after perihelion, where outbursts occurred, suggests that this weighting of the outburst signal did not distort the overall picture of high-activity areas presented by Läuter et al. (2019). This is supported by the steady increase in the overall CO_2/H_2O ratio seen in our data when the spacecraft was in Southern latitudes (see quiescent coma behaviour of the signal in Figs A1 and A2).

The source locations of H_2O and O_2 follow the subsolar latitude and correlate with each other. Notably, H_2O displayed high activity in these regions during summer 2015, while only a few summer fireworks events showed an increase in H_2O compared to highly volatile species. The high and confined activity of H_2O in the same areas as CO_2 around perihelion would decrease the CO_2/H_2O ratio if it was merely an artefact of the generally CO_2-rich outgassing of the outburst source regions.

A typical event is the one on 2015 July 28 (#5 in Vincent et al. 2016a). It is located in high-activity area 3 in Läuter et al. (2019), which was not among the most CO_2-rich areas during perihelion. Nevertheless, the CO_2/H_2O ratio exhibited a pattern for this event as for events in more CO_2-active areas, and comparable enhancements in 67P's coma were determined (Fig. 1 and Table A1).

When comparing the CO emission of the nine high-activity areas presented in Läuter et al. (2019) to the emission of H_2O, CO_2, and O_2, the CO signal is much more distributed and diluted during perihelion compared to the very localized outgassing of the other species. Thus, one would expect that the ratio of CO to H_2O should not increase much when measured in one of the high-activity areas. Nevertheless, our results show an enhancement of CO. In summary, most summer fireworks outburst events originate from generally CO_2-rich sources, however, they are clearly contributing an additional amount of highly volatile species to the overall outgassing behaviour.

The events described in Noonan et al. (2021) have been located close to the summer fireworks' source regions. The ROSINA/DFMS data also show gas density enhancements for CO_2 and CO. The

volatile enhancement in the outburst gas supports the scenario of pockets of gas in those areas and shows that the related activity is independent of the subsolar latitude (Läuter et al. 2019).

Unlike the events described by Noonan et al. (2021) and most of the events in Vincent et al. (2016a), the events reported by Grün et al. (2016), Agarwal et al. (2017), and the first event investigated by Feldman et al. (2016) show a large increase in H_2O with no CO_2 or CO enhancement. These outbursts showed short-lived H_2O enhancements, suggesting that they have been triggered by a different mechanism than the CO_2 outbursts – most likely by a cliff collapse as could be shown by Pajola et al. (2017). This conclusion is supported by the suggestion by Grün et al. (2016) that thermal stress in the surface material may have triggered a landslide (Fig. 7a) that exposed fresh H_2O ice to direct solar illumination (Fig. 7b).

It is prudent to note that the available set of outburst events is relatively small and confined to one individual comet. Furthermore, the measurement conditions, while corrected to the best of our abilities, varied for each event. The significant disparities observed in the distribution and temporal evolution of activity on cometary nuclei suggest that the heliocentric evolution of activity can be highly individual for each comet (Marschall et al. 2020a), and generalizations might be misleading. Moreover, given the large temporal differences between the outburst behaviour of the dust and the gas components, only their combined analysis provides a comprehensive view of the nature of the outbursts and their trigger mechanisms.

5 CONCLUSION

We conclude that outbursts appear due to two different mechanisms depending on their source location and associated surface topography. These mechanisms can be differentiated by their respective and distinct outgassing behaviour. Landslides or cliff collapses may cause an outburst event which would most probably be a water-driven event as fresh water ice would be found closer to the surface than, e.g. CO_2, and hence would be more exposed to solar illumination. However, most reported outburst events during the perihelion passage correlate with an increased composition of highly volatile species, especially CO_2, and generally higher activity source regions (Läuter et al. 2019). These events are most likely triggered by break-up of subsurface pockets of volatiles when the pressure inside overcomes the tensile strength of the cavity boundary layers. From these pockets, gas may seep out from smaller cracks already before the dust outburst as a slow increase in highly volatile species has been measured already before the dust ejection occurred. The surface and near-surface layers of the comet exhibit a general depletion in more volatile species, such as CO_2. This depletion may provide an explanation for the distinction between events dominated by H_2O and CO_2. H_2O events typically arise from occurrences in the surface or near-surface layers, while CO_2 events are likely to originate from greater depths where CO_2 did not yet find a way to evaporate freely. This distinction may highlight the influence of depth on the compositional characteristics of cometary outburst events. Nevertheless, in both cases, the exposure of fresh material implies extended enhanced outgassing after the dust outburst already ceased.

The unique temporal coverage of 67P's outgassing throughout the *Rosetta* mission has allowed a thorough analysis of the evolution and composition of the outgassing for more than 40 outburst events. The results indicate that the composition is linked to different trigger mechanisms, one related to cliff collapse, where water dominates the outgassing pattern, and pressure cooker-like ruptures of subsurface pockets, which are characterized by a strong enhancement of highly volatile species such as CO_2. These results are relevant for understanding changes in the outgassing patterns of comets from ground-based and *in situ* observations. However, open questions remain, such as the direct correlation between the different temporal behaviour of the dust and gas components of outbursts and the heliocentric distance dependence of the different triggering mechanisms for outbursts. Answering these questions requires further laboratory studies, sophisticated numerical simulations, observations, and missions monitoring a comet with high-resolution instruments over a prolonged time to gain a full understanding of cometary outbursts.

ACKNOWLEDGEMENTS

We thank the referee for the constructive feedback that enabled us to significantly improve the quality of the manuscript. We gratefully acknowledge the work of the many engineers, technicians, and scientists involved in the *Rosetta* mission and in the ROSINA (Rosetta Orbiter Spectrometer for Ion and Neutral Analysis) instrument in particular. Without their contributions, ROSINA would not have produced such outstanding results. *Rosetta* is an European Space Agency (ESA) mission with contributions from its member states and the National Aeronautics and Space Administration (NASA). Work at the University of Bern was funded by the State of Bern and the Swiss National Science Foundation (200020_207312). SFW acknowledges the financial support of the SNSF Eccellenza Professorial Fellowship (PCEFP2_181150).

DATA AVAILABILITY

All *Rosetta*/ROSINA data are available through the NASA Planetary Data System (PDS) and ESA's Planetary Science Archive (PSA).

REFERENCES

Agarwal J. et al., 2017, MNRAS, 469, s606
Altwegg K. et al., 2015, Science, 347, 1261952
Altwegg K., Balsiger H., Fuselier S. A., 2019, ARA&A, 57, 113
Altwegg K. et al., 2020, Nat. Astron., 4, 533
Altwegg K. et al., 2022, MNRAS, 516, 3900
Balsiger H. et al., 2007, Space Sci. Rev., 128, 745
Belton M. J. S., Feldman P. D., A'Hearn M. F., Carcich B., 2008, Icarus, 198, 189
Belton M. J. S. et al., 2013, Icarus, 222, 477
Bieler A. et al., 2015, Nature, 526, 678
Biver N. et al., 2019, A&A, 630, A19
Bockelée-Morvan D. et al., 2017, MNRAS, 469, S443
Bockelée-Morvan D. et al., 2022, A&A, 664, A95
Boogert A. C. A., Gerakines P. A., Whittet D. C. B., 2015, ARA&A, 53, 541
Calmonte U. et al., 2016, MNRAS, 462, S253
Combi M. R., Tenishev V. M., Rubin M., Fougere N., Gombosi T. I., 2012, ApJ, 749, 29
Crovisier J., 1999, in Greenberg J. M., Li A., eds, NATO Advanced Study Institute (ASI) Series C Vol. 523, Formation and Evolution of Solids in Space. Springer, Dordrecht, p. 389
De Keyser J. et al., 2019, Int. J. Mass Spect., 446, 116232
Feldman P. D. et al., 2016, ApJ, 825, L8
Fulle M., Altobelli N., Buratti B., Choukroun M., Fulchignoni M., Grün E., Taylor M. G. G. T., Weissman P., 2016, MNRAS, 462, S2
Gasc S. et al., 2017, Planet. Space Sci., 135, 64
Graf S. et al., 2004, J. Geophys. Res. (Planets), 109, E07S08
Grün E. et al., 2016, MNRAS, 462, S220
Hänni N., Altwegg K., Combi M., Fuselier S. A., De Keyser J., Rubin M., Wampfler S. F., 2022, Nat. Commun., 13, 3639
Hoang M. et al., 2019, A&A, 630, A33

Hughes D. W., 1975, Q. J. R. Astron. Soc., 16, 410
Hughes D. W., 1991, in Newburn R. L., Jr., Neugebauer M., Rahe J., eds, Astrophysics and Space Science Library Vol. 167, IAU Colloq. 116: Comets in the post-Halley era. Springer, Dordrecht, p. 825
Ip W.-H. et al., 2016, EGU General Assembly Conference Abstracts, EGU General Assembly Conference Abstracts, EPSC2016
Ishiguro M. et al., 2014, ApJ, 787, 55
Ishiguro M. et al., 2016, AJ, 152, 169
Jewitt D., Hui M.-T., Mutchler M., Weaver H., Li J., Agarwal J., 2017, ApJ, 847, L19
Kaufmann E., Attree N., Bradwell T., Hagermann A., 2020, J. Geophys. Res. (Planets), 125, e06217
Knollenberg J. et al., 2016, A&A, 596, A89
Kouchi A., Sirono S.-i., 2001, Geophys. Res. Let., 28, 827
Läuter M., Kramer T., Rubin M., Altwegg K., 2019, MNRAS, 483, 852
Le Roy L. et al., 2015, A&A, 583, A1
Lin Z.-Y., 2023, PASJ, 75, 462
Lin Z.-Y., Lin C.-S., Ip W.-H., Lara L. M., 2009, AJ, 138, 625
Lin Z.-Y. et al., 2017, MNRAS, 469, S731
Marschall R. et al., 2020a, Space Sci. Rev., 216, 130
Marschall R., Liao Y., Thomas N., Wu J.-S., 2020b, Icarus, 346, 113742
Meech K. J. et al., 2009, Icarus, 201, 719
Mellon M. T., 1997, J. Geophys. Res., 102, 25617
Noonan J. W. et al., 2021, AJ, 162, 4
Pajola M. et al., 2017, Nat. Astron., 1, 0092
Portyankina G., Merrison J., Iversen J. J., Yoldi Z., Hansen C. J., Aye K. M., Pommerol A., Thomas N., 2019, Icarus, 322, 210
Prialnik D., Jewitt D., 2022, preprint (arXiv:2209.05907)
Prialnik D., A'Hearn M. F., Meech K. J., 2008, MNRAS, 388, L20
Rinaldi G. et al., 2018, MNRAS, 481, 1235
Rubin M. et al., 2019, MNRAS, 489, 594
Rubin M. et al., 2023, MNRAS, 526, 4209
Samarasinha N. H., 2001, Icarus, 154, 540
Scherer S. et al., 2006, Int. J. Mass Spect., 251, 73
Schläppi B. et al., 2010, J. Geophys. Res. (Space Physics), 115, A12313
Schmitt M. I. et al., 2017, MNRAS, 469, S380
Shinnaka Y., Ootsubo T., Kawakita H., Yamaguchi M., Honda M., Watanabe J.-i., 2018, AJ, 156, 242
Sierks H. et al., 2015, Science, 347, aaa1044
Skorov Y. V., Rezac L., Hartogh P., Bazilevsky A. T., Keller H. U., 2016, A&A, 593, A76
Steckloff J., Melosh H. J., 2016, AAS/Division for Planetary Sciences Meeting Abstracts #48, 206.06
Thomas N. et al., 2019, Space Sci. Rev., 215, 47
Tubiana C. et al., 2015, A&A, 573, A62
Tzou C.-Y., 2017, PhD thesis. University of Bern, Switzerland
Vincent J. B. et al., 2016a, MNRAS, 462, S184
Vincent J. B. et al., 2016b, A&A, 587, A14
Wierzchos K., Womack M., 2020, AJ, 159, 136

APPENDIX A: EXTENDED DATA

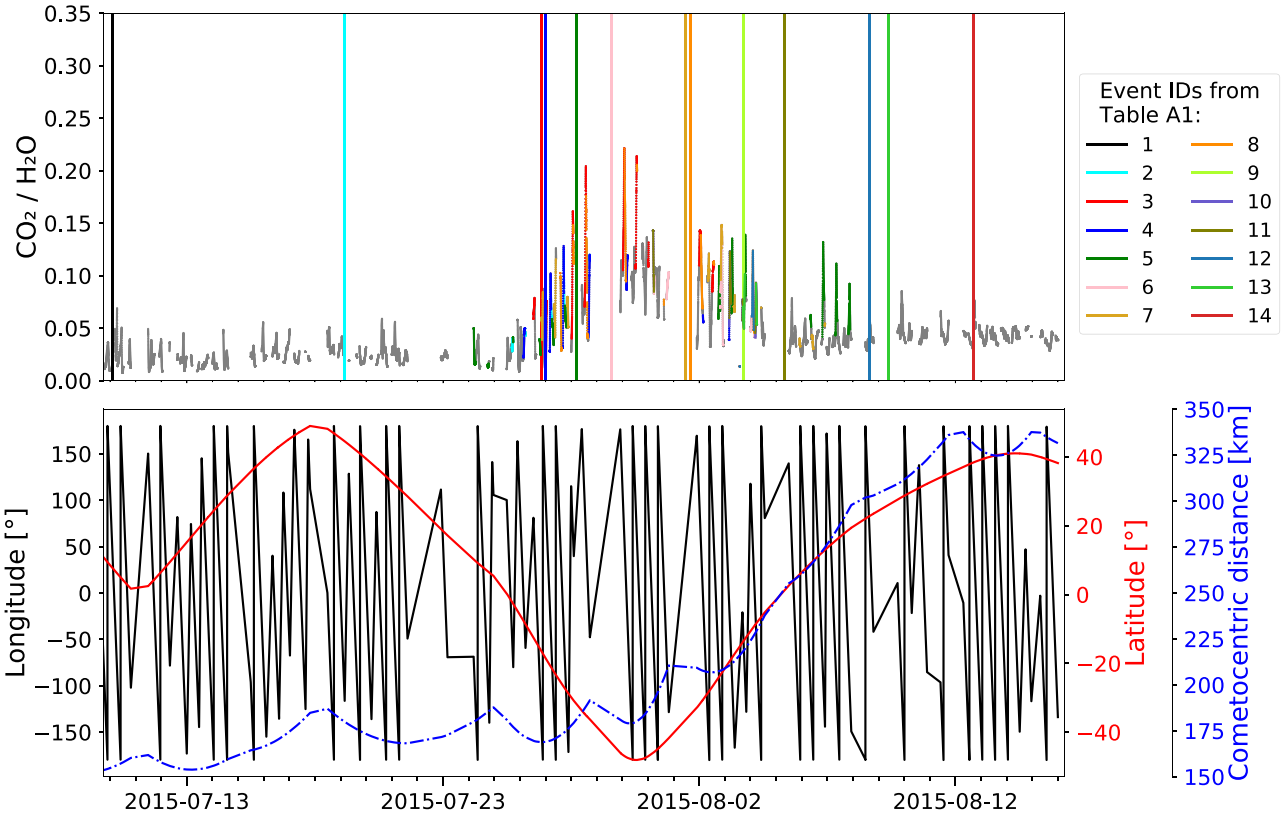

Figure A1. Top panel: Ion count ratio for CO_2 relative to H_2O for the first part of the summer fireworks from 2015 July 10 to August 17. The coloured data points show measurements taken when the *Rosetta* sub-spacecraft longitude and latitude was within 25° from the identified source location of the respective event. The vertical lines show the times when the events were detected by one of *Rosetta*'s cameras (Event IDs according to Vincent et al. 2016a, see Table A1). Bottom panel: Spacecraft longitude, latitude, and distance to the comet for the same time frame.

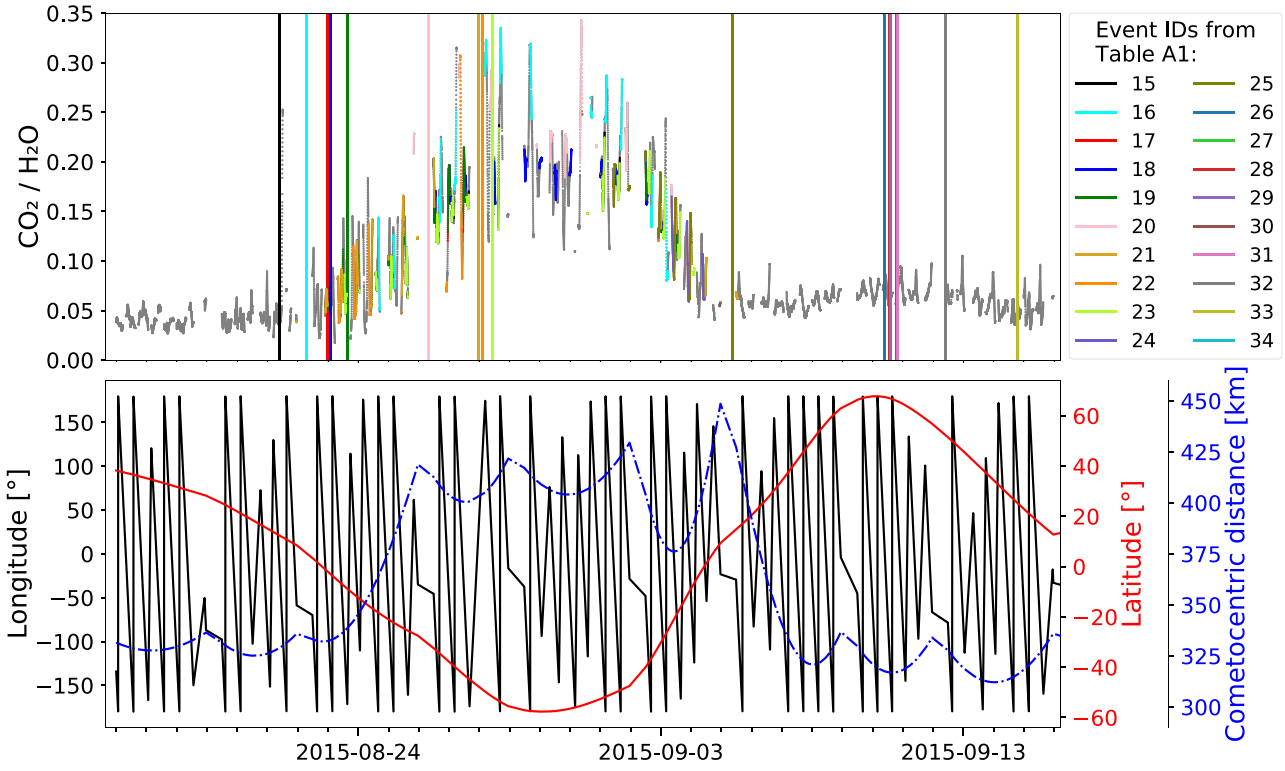

Figure A2. The same as in Fig. A1 but for the second part of the summer fireworks from 2015 August 16 to 2015 September 16.

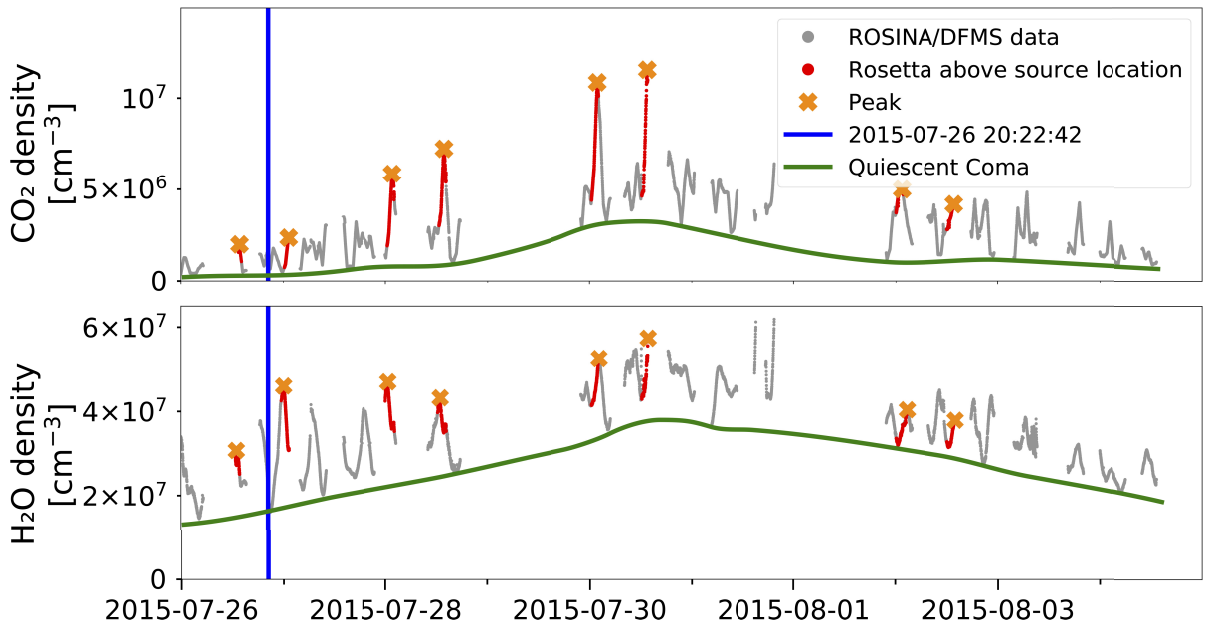

Figure A3. Typical ROSINA/DFMS densities of CO_2 and H_2O from 2015 July 26 until 2015 August 4 to show the analysis approach for the event on 2015 July 26, 20:22 UTC. To calculate the enhancement each time *Rosetta* was above the source location (i.e. for all phases with red measurement points), the peak value (orange cross) of CO_2 has been selected and corrected to the quiescent coma (green line). The same has been done for H_2O for the time when CO_2 showed its maximum. The peak values are slightly shifted in time due to the mass scanning nature of the instrument. These time shifts, on the order of a few minutes, do not affect the enhancement calculations as the time-scales associated to passing above the active region is substantially longer. The enhancement is then calculated based on equation (1).

Table A1. Gas density enhancements in the coma of 67P of the summer fireworks events (Vincent et al. 2016a). Most of these events were CO_2 dominated. For the few H_2O dominated events, density enhancements <1 mean that H_2O was the most dominant driver for the considered event and the enhancement of H_2O would be the inverse of the given value. Uncertainties on the enhancements are ±18 per cent, mostly due to instrument calibration uncertainties (Le Roy et al. 2015; Calmonte et al. 2016).

ID	Event Date (UTC)	cdist (km)	Lat (deg)	Lon (deg)	Time since sunrise (h)	CO_2	CO	O_2	H_2S	NH_3	CH_4	H_2CO	C_2H_6	CH_3OH	HCN	C_3H_8
1	2015-07-10T02:10:18	155	74	200	3.62	No observation										
2	2015-07-19T03:38:09	180	−24	296	3.09	8.3	1.8	0.7	3.1	2.3	3.3	3.4	9.8	3.7	4.0	13.5
3	2015-07-26T20:22:42	168	−36	75	11.16	19.7	7.1	0.7	4.0	2.7	9.7	6.1	26.9	12.2	8.8	18.5
4	2015-07-27T00:14:29	168	−31	333	10.24	21.8	12.1	1.6	4.3	6.6	8.2	3.5	26.2	9.6	7.8	22.6
5	2015-07-28T05:23:43	181	−4	264	10.73	6.9	2.2	0.9	2.7	2.6	3.1	3.4	7.3	3.5	3.3	13.5
6	2015-07-29T13:25:28	186	−37	300	3.69	18.8	5.3	0.8	3.8	4.2	3.5	2.9	21.2	9.6	3.6	20.6
7	2015-08-01T10:53:15	214	−12	196	10.51	13.8	5.7	0.8	2.1	3.2	3.5	2.9	17.7	7.7	6.4	12.4
8	2015-08-01T15:44:50	211	−28	34	10.68	16.1	4.9	2.2	4.1	2.5	4.5	3.5	13.6	6.1	4.5	12.9
9	2015-08-03T17:27:03	218	−75	303	9.97	2.2	0.4	1.1	1.4	0.9	0.7	0.3	2.3	1.1	1.2	N/A
10	2015-08-05T07:25:05	253	−25	320	10.32	23.9	6.7	2.3	4.3	4.8	3.6	3.4	16.6	6.2	6.3	16.7
11	2015-08-05T08:05:15	253	−23	318	10.47	Indistinguishable from #10										
12	2015-08-08T15:21:48	303	−30	51	3.41	14.0	4.9	2.2	2.8	2.5	4.5	3.5	13.6	6.1	4.5	12.9
13	2015-08-09T09:15:14	304	−30	298	9.94	6.9	6.2	2.3	1.9	2.2	3.3	3.3	15.5	5.9	5.7	16.4
14	2015-08-12T17:21:20	332	−30	58	3.32	0.6	0.2	0.2	0.6	0.7	2.5	0.4	1.6	0.7	0.3	N/A
15	2015-08-21T09:44:53	330	−32	227	10.61	4.1	1.7	1.1	1.2	2.1	1.3	1.8	4.9	2.1	2.4	5.4
16	2015-08-22T06:47:04	336	−40	168	3.15	24.3	14.0	1.8	4.2	5.4	7.8	6.2	20.5	7.9	5.1	23.3
17	2015-08-22T23:46:21	334	−25	316	11.60	18.7	6.8	2.1	1.7	2.3	4.8	1.2	19.1	4.4	4.8	13.6
18	2015-08-23T01:39:38	334	−53	292	3.33	4.3	3.3	2.1	1.6	6.9	4.8	3.5	6.6	2.1	3.8	4.2
19	2015-08-23T15:12:48	340	−23	314	3.28	Indistinguishable from #17										
20	2015-08-26T07:51:04	417	−41	42	10.43	15.1	11.1	1.9	2.3	1.7	6.7	2.5	9.8	4.7	4.4	10.6
21	2015-08-27T22:58:04	404	−8	321	10.76	18.7	4.5	0.7	1.8	2.5	1.6	1.5	16.8	2.0	5.9	13.6
22	2015-08-28T02:29:21	404	−21	24	3.07	5.1	1.7	1.0	1.3	1.4	1.6	1.8	4.2	2.1	1.6	5.0
23	2015-08-28T10:10:57	410	−31	229	3.63	4.1	1.0	2.6	2.9	2.5	1.3	4.5	2.5	1.8	5.7	5.4
24	2015-09-05T08:50:02	436	−15	26	11.63	No observation										
25	2015-09-05T09:00:02	435	−31	330	3.14	No observation										
26	2015-09-10T08:59:49	318	−25	67	3.33	No enhancements detected										
27	2015-09-10T13:06:14	317	−23	292	3.22	No enhancements detected										
28	2015-09-10T13:36:14	317	−21	307	3.46	No enhancements detected										
29	2015-09-10T14:11:15	317	−15	10	11.07	No enhancements detected										
30	2015-09-10T18:57:41	318	−15	10	9.93	No enhancements detected										
31	2015-09-10T19:27:41	318	−30	286	10.82	No enhancements detected										
32	2015-09-12T09:41:00	330	−12	318	11.44	1.0	1.1	0.8	1.2	1.7	1.7	2.0	1.1	0.5	0.7	N/A
33	2015-09-14T18:47:00	316	−25	198	3.36	0.9	0.4	1.0	1.5	0.8	0.6	0.8	1.1	1.5	0.4	N/A
34	2015-09-26T12:03:32	818	−40	307	10.47	DFMS Turned off										

This paper has been typeset from a TEX/LATEX file prepared by the author.